arXiv:1603.06662v1 [cond-mat.mes-hall] 22 Mar 2016

Stick-Slip Motion of the Wigner Solid on Liquid Helium

David G. Rees,[1,2,*] Niyaz R. Beysengulov,[2,3] Juhn-Jong Lin,[1,2,4] and Kimitoshi Kono[1,2,3]

[1] *NCTU-RIKEN Joint Research Laboratory, Institute of Physics, National Chiao Tung University, Hsinchu 300, Taiwan*
[2] *RIKEN CEMS, Wako 351-0198, Japan*
[3] *KFU-RIKEN Joint Research Laboratory, Institute of Physics, Kazan Federal University, Kazan, Russia*
[4] *Department of Electrophysics, National Chiao Tung University, Hsinchu 300, Taiwan*

(Dated: March 23, 2016)

We present time-resolved transport measurements of a Wigner solid (WS) on the surface of liquid Helium confined in a micron-scale channel. At rest, the WS is 'dressed' by a cloud of quantised capillary waves (ripplons). Under a driving force, we find that repeated WS-ripplon decoupling leads to stick-slip current oscillations, the frequency of which can be tuned by adjusting the temperature, pressing electric field, or electron density. The WS on liquid He is a promising system for the study of polaron-like decoupling dynamics.

PACS numbers: 73.20.Qt, 73.20.-r, 62.20.Qp

Surface-state electrons (SSEs) on liquid helium substrates (Fig. 1) form a model Coulomb system[1], the ground state of which remains the clearest example of the classical Wigner solid (WS)[2]. The WS is dressed by a cloud of ripplons, the Bragg scattering of which from the electron lattice gives rise to a commensurate deformation of the He surface known as the dimple lattice (DL)[3–6]. The WS-DL system is analogous to polaron states in which electrons are dressed by a cloud of virtual phonons, or lattice deformation[7–9]. On liquid He individual electrons do not perform self-trapping; rather, the DL appears as a consequence of the long-range electron ordering. Also, the lattice constant of the WS (and so the DL) is no less than 100 nm and a continuum description of the medium (liquid He) is applicable. Despite these differences, the decoupling dynamics of the WS and polaron systems exhibit strong similarities[10, 11], although the rate depends on the different binding energies; polaron decoupling in a GaAs crystal occurs in the femtosecond range[12], whereas the decoupling of the WS from the DL takes place on nanosecond timescales. It is therefore more straightforward to observe the real-time decoupling for the WS than for polarons.

In contrast with other systems, the coupling of the WS with the DL is of a dynamical nature, due to a resonant interaction between the WS and ripplons emitted by the moving electron lattice. According to hydrodynamic theory, when the WS is at rest the depth of the surface dimples ξ_0 can be estimated as

$$\xi_0 \approx -\frac{\sqrt{3}eE_z}{8\pi^2\sigma}e^{-W} \quad , \tag{1}$$

where e, E_z, σ and e^{-W} are the elementary charge, perpendicular pressing electric field, surface tension coefficient of liquid He and the self-consistent Debye-Waller factor, respectively[13]. Typically, $\xi_0 \approx 10^{-12}$ m. However, when the velocity of the WS-DL system approaches the phase velocity of ripplons of wavevector equal to the WS periodicity, v_{BC}, constructive interference resonantly deepens the DL. As a result, the resistive force exerted on the WS increases dramatically. This is called the Bragg-Cherenkov (BC) effect[14–16]. The decoupling of the WS therefore occurs from this dynamically pinned state and, hence, under strongly nonequilibrium conditions. So far, however, very little is known about this decoupling process. It is an interesting problem concerning strongly correlated systems far from equilibrium, and also from a hydrodynamics point of view.

The WS decoupling from the DL was first observed in Corbino conductivity measurements under perpendicular magnetic fields[17]. The decoupling was signalled by an abrupt jump in conductivity on sweeping the amplitude or frequency of the sinusoidal driving potential, or the magnetic field, or so on[18]. In such experiments, magnetic fields are necessary because an electric field large enough to cause the decoupling cannot be applied to the WS due to its high mobility. The electric current then flows azimuthally, whereas the electric field acts in the radial direction. The Hall angle is almost 90 degrees, and hence, the azimuthal current or velocity of the SSEs is extremely difficult to determine. Furthermore, the electric field is spatially inhomogeneous and time varying. These ambiguities make analysis of the decoupling process difficult.

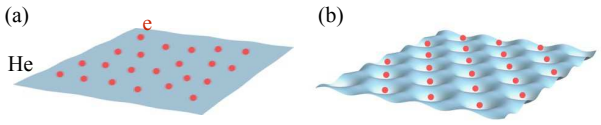

FIG. 1. (Color online) Schematic depiction of electrons on the surface of liquid helium. (a) Above T_m electrons move freely in the 2D plane above the surface. (b) Below T_m the Wigner solid is dressed by capillary waves, giving rise to the dimple lattice.

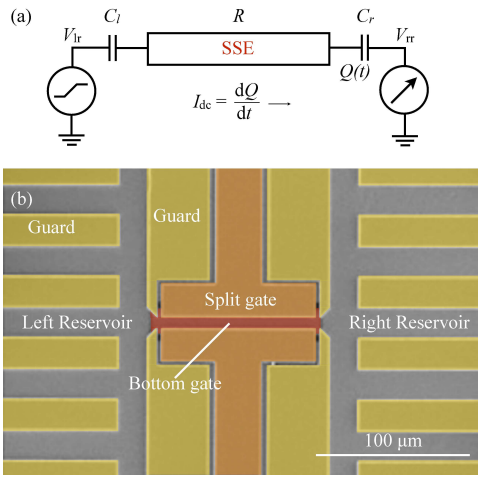

FIG. 2. (Color online) (a) Schematic circuit diagram of the dc current measurement. The SSE in the CM form an electrical resistance R. The electron system is coupled to the external circuit by the capacitances C_l and C_r. The current I_{dc} flows through the CM in response to varying V_{lr}, resulting in the transfer of charge $Q(t)$ from the left to the right reservoir, which accumulates in C_l and C_r. The capacitive coupling to the Guard electrode is omitted for simplicity. (b) False-colour scanning electron micrograph of a sample identical to those used in the experiment. The Left and Right Reservoirs each contain 25 microchannels of length 0.7 mm connected in parallel.

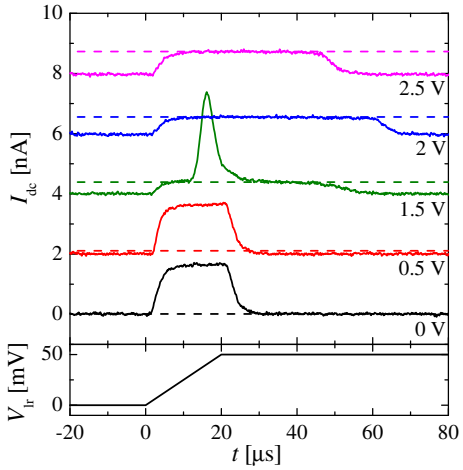

FIG. 3. (Color online) I_{dc} against time t for $V_{sg} = -0.2$ V and different values of V_{bg} as indicated on the plot. Here $T = 0.6$ K. Each data set is shifted vertically by 2 nA for clarity. The dashed lines indicate the value of I_{BC} expected for each value of V_{bg}. The lower panel shows the V_{lr} voltage waveform.

Recently, SSEs in capillary-condensed microchannel devices have been found to show the decoupling phenomena without applying magnetic fields[19]. In such devices the electric current is homogeneous but is typically measured using a sinusoidal driving voltage. The transport measurement is then inevitably complicated by the nonlinear response of the WS during each ac cycle. In this Letter we report simultaneous measurements of the WS velocity and driving electric field by employing a linear sweep of the driving electric potential. That is, we performed the first time-resolved transport measurement of a quasi-1D WS confined in a microchannel. We demonstrate that, under a driving potential, repeated ripplon dressing and decoupling causes stick-slip motion of the WS and so oscillations of the electron velocity. Our experiment allows the control and quantitative analysis of the decoupling dynamics of the WS.

The device used in the experiment is shown in Fig. 2(b). Our sample is electrons floating on a helium surface in a microchannel 7.5 μm wide, 100 μm long and $h = 2.2$ μm deep. We denote this the central microchannel (CM). Two large arrays of microchannels, which act as electron reservoirs, are attached to the CM. The SSE in the reservoirs are capacitively coupled to the external circuit by C_l and C_r, as shown schematically in Fig. 2(a). To measure SSE transport through the CM, the voltage V_{lr} applied to the electrode beneath the He in the left reservoir (Left Reservoir electrode) was ramped from 0 to +50 mV in a time t_r. As V_{lr} is varied, charge moves between the reservoirs. After the ramp period, the charge distribution achieves a new equilibrium state and the current stops. To determine the charge accumulated in C_l and C_r, and so the SSE current I_{dc} passing through the CM, the current flowing in the electrode beneath the He in the right reservoir (Right Reservoir electrode, $V_{rr} = 0$ V) was recorded. To tune the electrostatic confinement for SSEs in the CM, voltages V_{bg} and V_{sg} were applied to the electrode beneath the He in the CM (Bottom Gate electrode) and the electrode in the plane of the He surface (Split Gate electrode), respectively. The voltage on the Guard electrode was -0.2 V.

The current measurement was performed using a current preamplifier and a digital storage oscilloscope. The measurement was averaged over several thousand cycles. A small current component due to cross-talk between the electrical cables was subtracted from the measurement. The bandwidth of the preamplifier was 200 kHz, which leads to the smoothing of some of the transport features shown here but does not detract from the essential physics. Finite-element modelling (FEM)[20] was used to calculate the average areal electron density n_s (m^{-2}), the electrostatic potential of the electron system V_e (which depends on n_s), the effective width w_e of the charge sheet in the CM, the linear electron density n_l (m^{-1}), and the number of electron rows N_y, for varying bias conditions[21, 22].

Results of transient current measurements are shown in Fig. 3 for $t_r = 20$ μs, $V_{sg} = -0.2$ V. Generally, current flows in the CM in response to the V_{lr} ramp. However, the transport is strongly influenced by V_{bg}, the value of which determines the electron density in the CM. The

WS forms when the ratio of the electron Coulomb energy to kinetic energy $\Gamma = E_C/E_k = e^2\sqrt{\pi n_s}/4\pi\varepsilon_0 k_B T$ reaches a threshold value of ~ 130, where ε_0, k_B and T are the vacuum permittivity, the Boltzmann constant and the temperature, respectively[2]. At the experimental temperature $T = 0.6$ K the WS should form when $n_s \approx 7.1 \times 10^{12}$ m^{-2}, which occurs when $V_{bg} = 0.18$ V according to the FEM[22]. It is clear that for both the electron liquid ($V_{bg} = 0$ V) and the low-density WS ($V_{bg} = 0.5$ V) a constant current flows in the CM as V_{lr} changes. For $V_{bg} = 1.5$ V the current is initially suppressed but then suddenly increases, during the V_{lr} ramp, before relaxing. For $V_{bg} = 2.0$ V and 2.5 V, I_{dc} is small and continues to flow after the ramp phase.

Because the SSE system is capacitively coupled to both the Reservoir and Guard electrodes, the measurement of the current registered on the Right Reservoir electrode does not give the true current flowing in the CM. The average charge detected by integrating the current measurements shown in Fig. 3 is $Q^{av} = 1.58 \times 10^5 \cdot e$ with standard deviation $0.04 \times 10^5 \cdot e$. The FEM analysis gives the expected value $Q^{FEM} = 2.03 \times 10^5 \cdot e$. The deficit is due to the displacement current flowing into the Guard electrode. In Figs. 3 and 4, the current measurement is therefore corrected by the factor $Q^{FEM}/Q^{av} = 1.28$.

BC scattering followed by WS-DL decoupling results in an abrupt jump in the WS conductivity with increasing driving force. The influence of BC scattering on the WS velocity in the CM can be estimated using the periodicity of the WS along the channel, $a = N_y/n_l$. The limiting velocity is given by $v_{BC} = (\sigma k/\rho)^{1/2}$, where the wavevector $k = 2\pi/a$ and ρ is density of liquid He. The typical electron spacing is 300 nm, and therefore $kh \gg 1$. In this 'thick-film' limit the dispersion relation for ripplons on bulk liquid He $\omega^2 = (\sigma/\rho)k^3$ is applicable. The BC scattering-limited current was calculated as $I_{BC} = n_l e v_{BC}$ for the bias conditions in Figs. 3 and 4.

On comparing I_{BC} with the measurements in Fig. 3, it is clear that when V_{bg} is sufficiently large the WS is pinned to the DL and, due to BC scattering, $I_{dc} = I_{BC}$. Then, because I_{dc} is limited, the potential difference between the left and right reservoirs builds up during the V_{lr} ramp and the current continues to flow after the ramp phase. For $V_{bg} = 1.5$ V the electron velocity is initially limited by the BC scattering but, as the potential difference builds, suddenly increases when the electrons decouple from the DL. This releases the force and the electron velocity quickly returns to v_{BC}. For $V_{bg} = 0.5$ V the driving force always overcomes the weaker pinning and the current exceeds I_{BC}.

The stronger pinning of the WS with increasing V_{bg} is expected, as n_s (and so Γ) and E_z both increase with V_{bg}. However, by keeping the electrode bias conditions fixed and changing temperature, the influence of the electron thermal motion on the WS decoupling can be determined unambiguously. Approaching the WS melting point, thermal fluctuations in the electron positions should degrade the DL, leading to a decrease in the decoupling threshold force. This in turn should lead to a decrease in the time taken for the decoupling to occur in our transport measurements. In Fig. 4(a) we show I_{dc} against time t at different temperatures. Here $t_r = 80$ μs. The Split-Gate voltage was $V_{sg} = -1$ V which reduces n_s and w_e. This increases the resistance of the SSE system R and thereby slows the system response to the V_{lr} ramp (see Fig. 2(a)). During the ramp phase, multiple decoupling events occur, at regular intervals. After each decoupling event I_{dc} returns to I_{BC} and the stick-slip cycle is repeated. For increasing T (decreasing Γ) the stick-slip period decreases as the time taken to reach the decoupling threshold force is reduced.

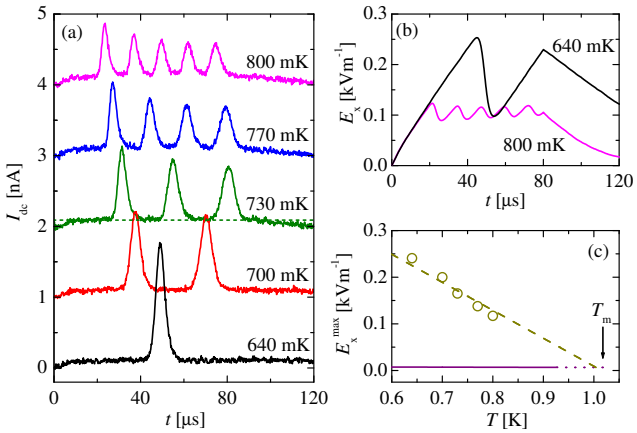

FIG. 4. (Color online) (a) I_{dc} against time t at different temperatures from 640 mK to 800 mK, as indicated on the plot. Here $t_r = 80$ μs, $V_{bg} = 1.2$ V and $V_{sg} = -1$ V. Each data set is shifted by 1 nA for clarity. For $T = 730$ mK, we plot the expected I_{BC} (dashed line). (b) E_x against t for the data shown in (a) for $T = 640$ mK and 800 mK. (c) E_x^{max} against T, for the data shown in (a). The dashed line is a guide to the eye. The solid/dotted line indicates the value of E_x^{max} expected for a dimple depth ξ_0. $T_m = 1.02$ K is indicated by the arrow.

Similar narrow-band current oscillations, also attributed to WS sliding, have been observed for degenerate electron systems in the WS regime[23]. However, for such cases little is known about the nature of the collective electron ground states or the mechanisms by which pinning forces are overcome. Qualitatively similar phenomena are observed in charge/spin density wave systems. But, contrary to those systems, the present system does not have a pinning mechanism due to irregularities. In our experiments, the quantitative understanding of the BC scattering mechanism allows us to clearly demonstrate the link between WS sliding and the appearance of spontaneous current oscillations.

Stick-slip motion typically results in a saw-tooth-type force-velocity profile[24]. For the data shown in Fig. 4(a), to calculate the time-varying electric field along

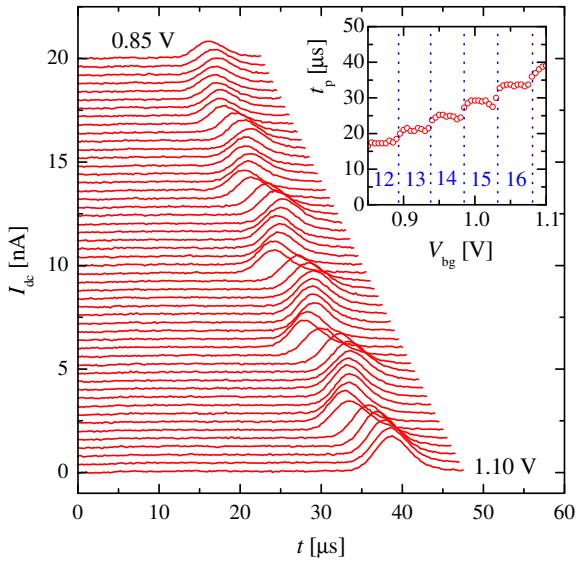

FIG. 5. (Color online) I_{dc} against t for different values of V_{bg}. V_{bg} is varied from 1.10 to 0.85 V in 5 mV steps. Each data set is shifted by 0.4 nA for clarity. Inset: the corresponding values of the I_{dc} peak position, t_p, against V_{bg}. The dotted lines mark the values of V_{bg} at which structural transitions between electron row configurations occur, as calculated by the FEM. The values of N_y between each transition are indicated.

the CM, $E_x(t)$, we integrate I_{dc} at each value of t to obtain the charge accumulated in the right reservoir $Q(t)$. Analysis of the circuit diagram in Fig. 2(a) gives $E_x(t) = [V_{lr}(t) - V_{rr} - 2Q(t)/C]/l$, where $l = 100$ μm and $C = C_l = C_r = 1.01$ pF is given by the measurement of Q_{av}. In Fig. 4(b) we show the dependence of E_x on t, at $T = 800$ and 640 mK. The driving field builds steadily when the WS is pinned by the DL and then drops rapidly as the WS decouples. The maximum value of the driving field E_x^{max} is higher at lower temperature, as expected. For this measurement, the FEM gives $n_s = 2.04 \times 10^{13}$ m^{-2}, for which the melting temperature $T_m = 1.02$ K. As shown in Fig. 4(c), E_x^{max} extrapolates close to this value, as the decoupling force becomes zero when the WS melts.

Assuming a sinusoidal surface profile, equating the components of the forces acting on each electron in the direction of motion yields the expression $k\xi_{th} = E_x^{max}/E_z$, where ξ_{th} is the dimple depth at the decoupling threshold. The E_x^{max} expected for the static DL ($\xi_{th} = \xi_0$) is shown in Fig. 4(c). (Note that the dependence of ξ_0 on T is weak, without taking the WS melting into account). As expected, the experimental values of E_x^{max} are larger than those for the static DL, as a consequence of the resonant deepening of the DL due to BC scattering. For $T = 0.64$ K, we estimate $E_x^{max}/E_z = 1.4 \times 10^{-3}$, $a = 240$ nm, and so $\xi_{th} = 5.2 \times 10^{-11}$ m. This value exceeds the static dimple depth $\xi_0 \approx 2 \times 10^{-12}$ m, and is consistent with other measurements[19].

For the bulk 2D WS the magnitude of the WS-DL coupling is estimated by $eE_z\xi_0$ (Eq. (1)). Since E_z and W are functions of V_{bg}, the decoupling threshold depends on V_{bg}, yet the dependence should be monotonous and smooth. In Fig. 5 we show I_{dc} against t, recorded for V_{bg} values between 0.85 and 1.10 V. Here $t_r = 80$ μs, $V_{sg} = -1$ V and $T = 0.6$ K. The time values at which I_{dc} reaches its peak value, t_p, are plotted in the inset. Although the general trend, the increase of the decoupling threshold, is as expected, it is remarkably tortuous. We ascribe this effect to successive structural transitions of electron row formation. The numbers of electron rows along the quasi-1D channel, as calculated by the FEM, are indicated in the inset of Fig. 5. Clear correspondence is observed. Previous (ac) measurements have shown a similar modulation effect due to the reduced positional order of the WS at each structural boundary[21, 25]. Further details of the influence of confinement on the WS ordering will be reported elsewhere.

Stick-slip motion is common in nature, although complex microscopic processes often determine macroscopic motion[26–28]. Here, for SSEs in a microchannel confinement, we have demonstrated a quantitative understanding of stick-slip friction at a microscopic level and that the coupling between the WS and the He substrate depends on the positional ordering of the quasi-1D electron system. Recently, quasi-1D cold ion systems comprising less than 10 particles have been used to investigate the influences of dimensionality and commensurability on sliding friction[29]. Our results demonstrate that similar investigations can be conducted with quasi-1D SSE systems, which can contain a much larger number of particles, by measuring decoupling from the DL or from lithographically structured substrates.

In conclusion, we have presented the first demonstration of stick-slip motion of the WS on a liquid He substrate. Our microchannel device allows precise control and quantitative analysis of the WS decoupling, which exhibits basic similarities with polaron dynamics. SSEs on He are a promising system to study stick-slip friction at the nanoscale.

We are grateful to M. I. Dykman for helpful discussions. This work was supported by JSPS KAKENHI Grant No. 24000007, and by the Taiwan Ministry of Science and Technology (MOST) through Grant Nos. NSC 102- 2112-M-009-015 and MOST 103-2112-M-009-017 and the the MOE ATU Program. This work was performed according to the Russian Government Program of Competitive Growth of Kazan Federal University.

* drees@nctu.edu.tw

[1] E. Y. Andrei, ed., *Two-dimensional electron systems*

on helium and other cryogenic substrates. (Kluwer Academic, Dordrecht, 1997).
[2] C. C. Grimes and G. Adams, Phys. Rev. Lett. **42**, 795 (1979).
[3] Y. P. Monarkha and V. B. Shikin, Sov. Phys. JETP **41**, 710 (1975).
[4] D. S. Fisher, B. I. Halperin, and P. M. Platzman, Phys. Rev. Lett. **42**, 798 (1979).
[5] M. Saitoh, J. Phys. Soc. Jpn. **55**, 1311 (1986).
[6] P. Leiderer, W. Ebner, and V. B. Shikin, Surface Science **113**, 405 (1982).
[7] A. S. Alexandrov and J. T. Devreese, *Advances in polaron physics* (Springer, 2010).
[8] M. I. Dykman and E. I. Rashba, Physics Today **68**, 10 (2015).
[9] E. Y. Andrei, Phys. Rev. Lett. **52**, 1449 (1984).
[10] A. A. Johansson and S. Stafström, Phys. Rev. B **69**, 235205 (2004).
[11] N.-H. Ge, C. Wong, R. Lingle, J. McNeill, K. Gaffney, and C. Harris, Science **279**, 202 (1998).
[12] P. Gaal, W. Kuehn, K. Reimann, M. Woerner, T. Elsaesser, and R. Hey, Nature **450**, 1210 (2007).
[13] Y. P. Monarkha and K. Kono, J. Phys. Soc. Jpn. **74**, 960 (2005).
[14] M. I. Dykman and Y. G. Rubo, Phys. Rev. Lett. **78**, 4813 (1997).
[15] W. F. Vinen, J. Phys.: Condens. Matter **11**, 9709 (1999).
[16] A. Kristensen, K. Djerfi, P. Fozooni, M. J. Lea, P. J. Richardson, A. Santrich-Badal, A. Blackburn, and R. W. van der Heijden, Phys. Rev. Lett. **77**, 1350 (1996).
[17] K. Shirahama and K. Kono, Phys. Rev. Lett. **74**, 781 (1995).
[18] K. Shirahama and K. Kono, J. Low Temp. Phys. **104**, 237 (1996).
[19] H. Ikegami, H. Akimoto, and K. Kono, Phys. Rev. Lett. **102**, 046807 (2009).
[20] F. Hecht, J. Numer. Math. **20**, 251 (2012).
[21] N. R. Beysengulov, D. G. Rees, Y. Lysogorskiy, N. K. Galiullin, A. S. Vazjukov, D. A. Tayurskii, and K. Kono, J. Low Temp. Phys. **182**, 28 (2016).
[22] See Supplemental Material at for details of the experimental method, electrostatic modelling and ac transport measurements used to characterise the device.
[23] G. A. Csáthy, D. C. Tsui, L. N. Pfeiffer, and K. W. West, Phys. Rev. Lett. **98**, 066805 (2007).
[24] B. N. J. Persson, *Sliding friction: physical principles and applications*, Vol. 1 (Springer Science & Business Media, 2000).
[25] H. Ikegami, H. Akimoto, D. G. Rees, and K. Kono, Phys. Rev. Lett. **109**, 236802 (2012); D. G. Rees, H. Ikegami, and K. Kono, J. Phys. Soc. Jpn. **82**, 124602 (2013).
[26] A. Vanossi, N. Manini, M. Urbakh, S. Zapperi, and E. Tosatti, Rev. Mod. Phys. **85**, 529 (2013).
[27] C. Lee, Q. Li, W. Kalb, X.-Z. Liu, H. Berger, R. W. Carpick, and J. Hone, Science **328**, 76 (2010).
[28] M. Lee, B. Kim, J. Kim, and W. Jhe, Nature communications **6** (2015).
[29] A. Bylinskii, D. Gangloff, and V. Vuletić, Science **348**, 1115 (2015).

SUPPLEMENTAL - MATERIALS AND METHODS

The sample was fabricated on a silicon wafer using optical lithography. Two gold layers, each 80 nm thick, were separated by an insulating layer of hard-baked photoresist. The metal layers were patterned to form the different electrodes. The widths of the gaps between the electrodes were approximately 0.5 μm in the lower layer and 3 μm in the upper layer. After lift-off of the second layer, the photoresist that was not covered by metal was removed by etching to form the channel structures. The reservoirs comprised 25 microchannels, each 20 μm wide and 700 μm long, connected in parallel.

The samples were wire bonded to a ceramic chip carrier that was then mounted in a hermetically sealed copper sample cell attached to the mixing chamber of a dilution refrigerator. ^{4}He was condensed into the sample cell until the surface of the superfluid was approximately 0.5 mm below the sample, allowing the microchannels to fill by the capillary action of the superfluid film. A 100 ms voltage pulse was applied to a tungsten filament placed several mm above the sample to induce the thermal emission of electrons. The charging procedure was performed at 0.9 K, at which temperature the electrons thermalise rapidly due to collisions with He gas atoms before being trapped on the surface.

Ac transport measurements, in which the driving force applied to the SSE can be made very small, were performed by superimposing a small ac voltage V_{in} on the Left Reservoir electrode and measuring the ac current I_{ac} induced in the Right Reservoir electrode, using the current preamplifier and a lock-in amplifier. The ac frequency was 89.2 kHz.

SUPPLEMENTAL - AC TRANSPORT MEASUREMENTS AND FINITE ELEMENT MODELLING

Before investigating the dc transport, we performed ac transport measurements, and used the results to build an electrostatic model of the device with the aid of finite element modelling (FEM). We first measured the Split-Gate voltage threshold of current flow V_{sg}^{th} for different values of V_{bg}. The results of the measurement are shown in Fig. 1(a) for $V_{gu} = -0.2$ V, $V_{lr} = V_{rr} = 0$ V and $V_{in} = 3$ mV$_{pp}$. For such small driving voltage, the system remains close to equilibrium during the measurement. For increasingly positive V_{bg}, a more negative V_{sg} is required to 'pinch-off' the current. At this threshold, where electrons enter the CM forming a single row along the centre of the channel, two energetic conditions must be satisfied. Firstly, the potential at the centre of the CM, V_c, must be more positive than the electrostatic potential of the electron system V_e. Were the electron system to behave as a charge continuum, the satisfaction of this condition alone would result in current flow. However, because the electron system is granular in nature, a second condition arises, that the charging energy required to populate the CM with electrons must be compensated for. We consider that this condition is approximately satisfied when the number of electrons allowed in a square section of the effective CM area $S = w_e^2$ is equal to 1 or, equivalently, that the separation between the electrons along the centre of the CM is comparable to w_e.

We then used a finite element modelling software package[20] to solve Poisson's equation for the electrostatic potential ϕ at all points in the CM cross section, according to the geometry and bias conditions of the sample. Without electrons, the potential at the centre of the CM was given by $V_c = \alpha V_{bg} + \beta V_{sg}$, where α and β are coupling constants. (The influence of the other electrodes is negligible as they are strongly screened.) The electron system was then modelled as a continuous charge sheet of width w_e and potential V_e. The width was determined, for varying electrode bias conditions, by iteratively calculating the value of w_e for which the electric field at the edge of the sheet, in the plane of the helium surface, was zero. The surface charge density distribution across the electron sheet $n_s(y)$ was then found by measuring the difference between the electric field above and below the electron sheet, using the expression

$$\left.\frac{\partial\phi}{\partial z}\right|_{above} - \varepsilon_{He}\left.\frac{\partial\phi}{\partial z}\right|_{below} = \frac{-en_s(y)}{\varepsilon_0} \quad , \tag{2}$$

where ε_0 is the permittivity of free space and $\varepsilon_{He} = 1.056$ is the dielectric constant of liquid He. The average areal density n_s was given by the average value of $n_s(y)$ whilst the linear electron density n_l in the CM was evaluated numerically using the expression

$$n_l = \int_{\frac{-w_e}{2}}^{\frac{w_e}{2}} n_s(y)dy \quad . \tag{3}$$

The number of electron rows in the CM, N_y, was then estimated as $N_y = \sqrt{w_e n_l}$. Given our fabrication procedure, we expect a channel depth of approximately 2 μm. Using a channel depth of 2.2 μm, for which $\alpha = 0.6$ and $\beta = 0.4$, and the value $V_e = -0.13$ V we found an excellent agreement between the voltage values for which our model predicts $N_y = 1$ and the current threshold line, as shown in Fig. 1(a).

In Fig. 1(b) we show the dependence of I_{ac} on V_{bg} for two values of V_{in}. Here $T = 0.6$ K and the melting of the classical WS occurs for $n_s \approx 7.1 \times 10^8$ cm^{-2}. Our FEM model gives this value for n_s when $V_{bg} = 0.18$ V. For $V_{in} = 2$ mV$_{pp}$, the current drops abruptly close to this value as the WS couples with the DL. (In this regime, we also note the appearance of current oscillations as the

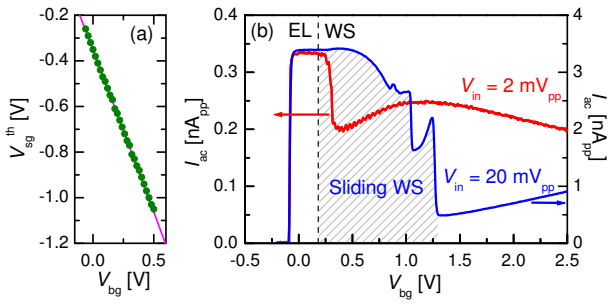

FIG. 6. Results of ac transport measurements. (a) V_{sg}^{th} against V_{bg} for $V_{lr} = V_{rr} = 0$ V, $V_{gu} = -0.2$ V, $V_{in} = 3$ mV$_{pp}$ and $T = 0.6$ K. The solid line shows the result of FEM modelling for $N_y = 1$. (b) I_{ac} against V_{bg} for $V_{gu} = V_{sg} = -0.2$ V and $V_{in} = 2$ and 20 mV$_{pp}$. The axes for the two measurements are scaled by a factor of 10 to allow clear comparison. The transition between the electron liquid (EL) and WS phases occurs when $V_{bg} \approx 0.18$ V. For $V_{in} = 20$ mV$_{pp}$ the WS 'slides' along the Helium surface before becoming pinned at $V_{bg} = 1.30$ V.

number of electron rows in the CM, and so the commensurability of the electron lattice with the confinement, is modulated. These effects will be described in detail elsewhere). For $V_{in} = 20$ mV$_{pp}$, the current remains high as the WS slides along the Helium surface, before the pinning with the DL occurs at $V_{bg} = 1.30$ V. In the sliding WS regime a current peak is observed immediately before the SSE are pinned by the DL. For $V_{in} = 20$ mV$_{pp}$, the root-mean-square rate of change of voltage is 3.9 mV/μs, comparable with the 2.5 mV/μs used in Fig. 3 in the main text. We therefore conclude that the current peak observed in the ac transport measurement arises due to WS sliding during each ac voltage cycle, resulting in a large signal component recorded at the ac reference frequency. Other resonances weakly observed in the ac measurement at lower values of V_{bg} occur when multiple sliding events occur during each cycle.